# Regional variation in digital cushion pressure in the forefeet of horses and elephants.

Horses and elephants have extreme foot designs; horses have an unguligrade foot posture with small, single-toed, rigid hooves housing a small fibrous digital cushion, whereas elephants have large, multi-toed, functionally plantigrade, compliant feet with large adipose filled digital cushions. The morphology of the digital cushion is divergent in these species, in terms of its size, shape, volume, composition and organisation. In the context of foot-ground contact this is interesting, because feet nonetheless have to perform similar mechanical functions in all terrestrial species. How well the digital cushion functions under load may contribute to the aetiopathogenesis of foot disease; a sub-optimal digital cushion is less likely to distribute (and thus reduce) high pressures, moderate impact shock and vibration, or prevent unwarranted bone displacement.

In this study, we seek to understand how the digital cushion morphologies evident in horse and elephant feet influence internal and external foot pressures. Our novel use of invasive blood pressure monitoring equipment, combined with a pressure pad and force plate, enabled measurements of (*ex vivo*) digital cushion pressure under increasing axial loads in seven horse and six elephant forefeet. Linear mixed effects models (LMER) revealed that internal digital cushion pressures increase under load and differ depending on region; elephant feet experienced higher magnitudes of medial digital cushion pressure, whereas horse feet experienced higher magnitudes of centralised digital cushion pressure. Direct comparison of digital cushion pressure magnitudes in both species, at equivalent loads relative to body weight, revealed that medial and lateral pressures increased more rapidly with load in elephant limbs. Within the same approximate region, internal pressures exceeded external, palmar pressures (on the sole of the foot), supporting previous Finite Element (FE) predictions. High pressures and large variations in pressure may relate to the development of foot pathology, which is a major concern in horses and elephants in a



*PeerJ PrePrints* | http://dx.doi.org/10.7287/peerj.preprints.231v1 | CC-BY 4.0 Open Access | received: 2 Feb 2014, published: 2 Feb 2014

captive/domestic environment.

We suggest that heterogeneity within the digital cushion allows it to perform conflicting mechanical functions during locomotion; different digital cushion regions may be responsible for specific functions and therefore feature appropriate properties to do so. Determining how internal structures such as the digital cushion respond to locomotor loading is essential to understanding foot health and pathology, as well as the functional consequences of evolutionary changes in foot morphology.



*PeerJ PrePrints* | http://dx.doi.org/10.7287/peerj.preprints.231v1 | CC-BY 4.0 Open Access | received: 2 Feb 2014, published: 2 Feb 2014

Sharon E. Warner[1*], Victoria Henry[1], Kyle Roskilly[1], Thomas Hildebrandt[2], Olga Panagiotopoulou[1,3], John R. Hutchinson[1].

[1]Structure & Motion Lab, Comparative Biomedical Sciences, The Royal Veterinary College, UK.
[2]Leibniz Institute for Zoo and Wildlife Research, im Forschungsverbund Berlin e.V., Postfach 601103, Berlin D-10252, Germany.
[3] School of Biomedical Sciences, Faculty of Medicine and Biomedical Sciences, The University of Queensland, Brisbane 4072, Australia.

* corresponding author:
Sharon Elaine Warner
Structure & Motion Laboratory, Department of Comparative Biomedical Sciences, The Royal Veterinary College, UK.
07919074135
swarner@rvc.ac.uk.

Keywords: foot, biomechanics, heel pad, locomotion, biomaterials.

## Introduction

Digital cushions are specialised fatty/fibrous pads (Wearing and Smeathers 2011) that protect bony prominences within the fore (manus) and hind feet (pes). As well as absorbing shock at foot impact, it has been proposed that these structures may distribute and thus reduce high, localised pressures (and loads) which can cause damage if their magnitudes exceed tissue safety thresholds. Mammalian digital cushion morphology shows a remarkable amount of variation (Egerbacher *et al.,* 2005; Weissengruber *et al.,* 2006; Raber *et al.,* 2004; Chi 2005; Ker 1999; Hsu *et al.,* 2007). Within the context of foot-ground contact, this is interesting because feet have to perform similar mechanical functions such as generating pressures against the substrate to support and propel the body (Alexander *et al.,* 1986; Chi and Roth 2010). Pressure is equal to force divided by area; therefore pressure can be moderated by reducing the force applied, or by increasing the surface area over which the force is applied. Although foot surface area increases with body mass, it may do so at a disproportionate rate, meaning that foot pressures are higher in larger mammals (Michilsens *et al.,* 2009). This study seeks to understand how extreme foot design influences internal and external foot pressures.

Horses and elephants are very similar in some respects; both are large, parasagittally striding, fairly straight-legged terrestrial quadrupeds, with long daily travel distances and grossly similar habitats (Carrano 1999; Hutchinson *et al.,* 2009). And yet, these two mammals have extremely different foot and digital cushion morphologies. Horses, as ultimate examples of unguligrades, have a fully erect foot posture whereby the most distal phalangeal bone supports body weight via the hoof (Douglas *et al.,* 1998; Bowker 2003); the carpal (or tarsal) bones, metapodials and phalanges are permanently raised off the ground (Fig. 1A). Their relatively small digital cushions (~13 % of total forefoot volume, Warner, 2014), have no discernible compartmentalisation and are contained within a rigid hoof capsule. Horse digital cushions are almost devoid of adipose tissue, instead containing dense connective, myxoid tissue and fibrous cartilage (Egerbacher *et al.,* 2005; Wilhelm *et al.,* 2005).

The opposing postural extreme is termed plantigrady, whereby the carpal (or tarsal) bones, metapodials and phalanges lie along the ground and with a system of digital and metacarpal/tarsal cushions, support body weight (Fig. 1B). Elephants are unusual in that they have a sub-unguligrade skeletal foot posture, but their digital cushion renders them functionally plantigrade, because the digital cushion (containing an enlarged strut-like “predigit”) directly supports body weight (Miller *et al.,* 2008; Hutchinson *et al.,* 2011).Their substantial digital cushions extend proximally from the sole to the metacarpals, providing almost 40 % of the foot’s total volume (Warner, 2014). Elephant digital cushions are formed of chambers of differing geometry filled with adipose tissue, with collagen, reticulin and elastic fibers also present (Weissengruber *et al.,* 2006).

How do these divergent digital cushion (and foot) morphologies mitigate high local pressures such as those experienced during foot impact or full weight support? Does the material composition of elephant digital cushions lead to greater compliance and viscosity compared to

horse digital cushions, meaning that they are better adapted to distributing and thus minimising high pressures (Panagiotopoulou *et al.,* 2012) and dampening impact forces (Aerts *et al.,* 1996; Warner et al., 2013)? And do supposedly disproportionate external foot pressures present a challenge to large animals with regards to foot health? As a first step towards these broader goals, here we focus on these two mammals in order to investigate how internal pressures change in horse and elephant digital cushions under load. Our study asks three principal questions, as follows.

First, does axial limb loading cause internal digital cushion pressures to change? Importantly, it is still unclear whether digital cushion pressures do change under load, due to the experimental difficulties associated with quantifying internal pressures. Invasive measurements of force are limited for ethical and practical reasons (e.g. animals might be least likely to move normally if their feet are subjected to surgical procedures), and despite finite element models indicating regional distributions of stress (Spears *et al.,* 2005; Luo *et al.,* 2011), these models are limited due the oversimplifications necessary to conduct the analysis. Considering that material testing of isolated (human heel pad) tissue samples have revealed variable results with regards to mechanical properties (DeClerq *et al.,* 1994; Aerts *et al.,* 1995), this study quantifies internal pressure (*in situ*) using *ex vivo* loading experiments of cadaveric forefoot material.

Previous work on horses *in vivo* (Dyhre-Poulsen *et al.,* 1994) suggested that limb loading induces negative digital cushion pressure (i.e., suction), however this study experienced substantial technical difficulties with transducer function. An increase of pressure induced by compression may be countered to some degree by the effects of medio-lateral and dorso-palmar foot expansion (Taylor *et al.,* 2005; Thomason *et al.,* 1992); however, the foot seems unlikely to expand to the extent needed to create negative pressure. For example, we calculated that if a load of 2500 N was applied (~50 % body weight), the digital cushion's cross sectional area would have to increase by > 5000 % to drop below zero pressure, relative to the unloaded limb. This suspicion provided additional motivation to re-examine horse digital cushion pressures in this study.

In both horses and elephants, the dorsal portion of the forefoot is contained-- either by the hoof capsule in horses or by the digits in elephants. Curiously, human heel pad (finite element) studies found that confining the heel pad reduced the predicted internal stress (Spears *et al.,* 2007). The palmar portion is, by comparison, more free to deform; hence digital cushion pressures in this region are more likely to be influenced by the extent of deformation. The primary hypothesis for this study is that internal digital cushion pressure will increase under load; further, because elephant digital cushions are likely to have greater compliance compared to horse digital cushions, equivalent loads (in terms of % body weight) will induce lower magnitudes of pressure change in elephant feet.

Second, do regional pressure differences exist within the digital cushion of horses or elephants? Previous studies on human heel pads indicate that the chambers present behave like fluid-filled sacs (Ker 1999); compressive loads cause pad deformation leading to displacement of adipose tissue, and tension in the fibrous septa between chambers and surrounding skin (Spears *et al.,* 2007). If the tissue within the chambers acts as an incompressible fluid, assuming constant volume, the pressure within each chamber should be uniform (Pascal's theory), assuming there is no fluid flow between the compartments (Jahss *et al.,* 1992).

Considering that elephants have differing chamber geometry (Weissengruber *et al.,* 2006), it is hypothesised that loading will cause differential pressure increases throughout the digital cushion

(specifically, macro-chamber pressures will increase with load at a lower rate than micro-chamber pressures). This is because the high ratio of fibrous septa: adipose tissue evident in micro-chambers (in contrast to macro-chambers) is likely to provide greater resistance to deformation (Hsu *et al.,* 2007). It is expected that pressures in these micro-chamber regions (which appear to be located more superficially from visually assessing high resolution MRIs, Warner, 2014, Fig, 2B) increase when small loads are applied, whereas pressures in macro-chamber regions will remain more stable until larger loads are applied.

Although horses lack discrete digital cushion chambers (visual assessment of high resolution MRIs, Warner, 2014, Fig. 2A), loading is expected to cause differential pressure increases throughout the cushion. Specifically, we hypothesise that pressure will increase to a greater degree in areas closest to the cushion's boundaries and in areas closer to points of compression.

Finally, how do external palmar and internal digital cushion pressures (in the same relative region) compare? Data from finite element models have predicted that internal pressures exceed external pressures (Spears *et al.,* 2007; Luo *et al.,* 2011), but this has not been determined experimentally. Here we compare synchronous pressure pad measurements of palmar pressure and internal digital cushion pressure measurements in cadaveric forefeet material for both study taxa.

## Materials and Methods

### Cadavers

A detailed list of subject information is in Table 1. Forelimbs, as opposed to hind limbs, were selected because forelimbs are under greater load in both species (Manter 1938; Jayes and Alexander 1978; Ren *et al*., 2010; Warner *et al*., 2013). Three horse (*Equus caballus* Linnaeus 1758) forelimbs were obtained from a local abattoir (Holts Purveyors of Fallen Stock, Stanstead Abbots, UK) and four more were obtained from the Royal Veterinary College's (RVC) Equine Hospital (post-mortem specimens). All had been euthanised for reasons other than musculoskeletal disease and unrelated to this study. All horses were adult, of mixed breeding, body masses 552 ± 95 kg (mean ± S.D.), 15 ± 10 years old. Limbs were frozen immediately after disarticulation and stored at - 20° C until they were thawed ready for use. Limbs were prepared as described by McGuigan and Wilson (2003). Shoes were removed if present and hooves were minimally trimmed (excess hoof wall was rasped level with the sole). Thawing took between 24-48 hours and all limbs had been at room temperature for at least six hours prior to data collection.

Elephant forelimbs were obtained from various zoo/safari park sources within the European Union (specimens from Hutchinson *et al.,* 2011). Four adult Asian elephant (*Elephas maximus* Linnaeus 1758) and two adult African elephant (*Loxodonta africana* Blumenbach 1797) limbs were obtained; estimated body masses 3532 ± 1052 kg (mean ± S.D.); 36 ± 16 years old. Elephants had died naturally or been euthanised for various health conditions; three limbs had obvious gross pathologies in the manual bones, but these had no apparent qualitative influence on the response of the digital cushion (see Data S1 for details of gross pathologies, Fig. S2, S3 for details of individual variation in elephants; Fig. S4, S5 for details of individual variation in horses). There is no evidence in the current literature of differences in digital cushion morphology or properties in Asian or African elephant forefeet; we assume that both species are far more similar to each other than to horses in these parameters. All limbs had been disarticulated at the level of the carpus and had been stored at - 20° C until they were thawed ready for use. Laboratory temperature was approximately 16° C throughout the experiments; humidity was not controlled.

### Equipment

Internal pressure was quantified using invasive blood pressure monitoring apparatus equipped with four transducers (0.2 Hz; Logical®, Smiths Medical, Kent, UK). Data were displayed on a monitor (Datex Ohmeda, Southwest Medical Ltd, Bedfordshire, UK) and logged using custom-written Datex Logger software (v.1, Kyle Roskilly). External (palmar) pressure was measured using a pressure pad (25 Hz; 0.5m RS Footscan plate containing 4096 sensors, plus RS Footscan Gait Software; Olen, Belgium), while applied force was measured using a Kistler force platform (25 Hz; type 9287B, Kistler Instruments AG; Winterhur, Switzerland), plus custom written Labview software (v2009 SP1, National Instruments; Austin, TX). Limbs were loaded using a manually operated hydraulic loading ram (10 tonne capacity, Clarke Strong-Arm, Dunstable, UK), mounted to a custom built loading frame. The frame was securely bolted to the laboratory floor, which housed the force platform and pressure pad.

### Needle placement

The (internal) pressure system was validated using the SURE-CAL® integrity facility on each transducer. Individual lines were flushed with water to ensure they were free from air bubbles,

prior to needle insertion. Figs. 3, 4 show the intended pressure sampling (needle) locations in horse and elephant limbs respectively. Four BD spinal needles (quince type point, 18 GA 3.50 IN 1.2 x 90 mm) were used, and additionally a BD Angiocath™ needle (14 GA 5.25 IN 2.1 x 133 mm) was used for the deepest location in the elephant. Needle placement was verified using either radiographs (dorso-palmar 65 kV, 24 mA; lateral 70 kV, 24 mA, using a PX-15H from SMR Medical Imaging, UK) of horse feet, or CT scans (5 mm axial slice thickness, 140 kV, 200 mA, using a Lightspeed QX/i from GE Medical, UK) of elephant feet.

## Limb loading

In horse limbs, a 12 mm diameter hole was drilled through the elbow joint; in elephant limbs, the hole was drilled through the distal carpal bone row, into the third/fourth metacarpal. The loading ram's pin was inserted into the pre-drilled hole, and then foot placement was adjusted until loading generated a centre of pressure (CoP) that was central to the foot (assessed using the pressure pad, see Fig. S6 showing the experimental set up and Fig. S7, S8 for the location of the CoPs in each individual across all trials). Additionally, in the horse, the foot was positioned so that the metacarpal became vertical under load, following McGuigan and Wilson (2003). Once the pin was inserted, the ram's head rested on the surrounding bone, preventing the pin from driving deeper into the bone.

## Pressure measurement adjustments

Drift in the pressure channels was monitored for at least 10 minutes once needles were *in situ* and the foot was positioned centrally beneath the loading ram. Trials began once drift did not exceed $\pm$ 0.05 $mmHgs^{-1}$. To overcome differences in static pressure, all channels were zeroed; the measured change in internal pressure as a result of loading was therefore measured relative to zero pressure (enforced by zeroing, in the unloaded state via the Datex Ohmeda hardware).

## Trials

Each 12 minute trial consisted of three phases; baseline data were recorded during the initial five minutes, after which the limb was loaded (which took up to ~ 30 seconds, depending on the magnitude of the load). The limb remained loaded for two minutes, after which it was unloaded; data were then recorded for a further five minutes. Applied loads spanned 0-150% body weight (BW) in horse limbs and 0-60% BW in elephant limbs; total number of loads per limb did not exceed 20. Trial timings ensured the limb had at least 10 minutes rest in between applied loads. The lengthy nature of applying the load (via the manually operated ram), meant that the capture frequency of the pressure pad had to be set to 25 Hz (trial lengths were restricted to 1000 data points), and thus the force platform's recording frequency was set to match the pressure pad's. Since the ram could not replicate high physiological loading rates, the analysis focussed on internal and external pressure changes as a result of static loads only (i.e., data collected during loading/unloading did not form part of the analysis).

## Data Processing

All data were exported to Matlab (v.R2001b, Mathworks Inc, Natick, MA, USA) for custom analysis; raw (Kistler) force data were low-pass filtered (100 Hz single pole RC filter), zeroed and summed to get $F_x$, $F_y$ and $F_z$, although only vertical force ($F_z$) was used here. The pressure pad was calibrated with a person of known mass (as per the manufacturer's instructions); however, our preparatory tests showed that the pad did not consistently quantify the applied

force. A force correction value was therefore calculated using the force platform data to correct the force (and pressure) data from the pressure pad (see Data S9 for further details). Spatial registration of external pressure data was not necessary because the foot's position on the pad did not change in between trials.

Figure 5 shows the internal pressure data (recorded in digital cushion four locations) and the vertical force data for a typical trial: a horse limb loaded to 112 % BW (~6000 N). Both mean and maximum instantaneous pressures were recorded because previous studies have shown that both are important in pathological foot conditions (Jahss *et al.,* 1992). Mean internal digital cushion pressure change was calculated by subtracting the average pressure data (calculated over a 30 second period, grey shaded area in Fig. 5) before loading, from the average pressure data at full load. The maximum instantaneous internal pressure was identified as the highest peak in pressure following load application. Peak and average vertical forces as well as the rate of force application were also calculated and recorded.

In order to compare internal and external pressures in the same region, the coordinates of the needle tips within the digital cushion were obtained via radiographs or CT scans; the z coordinates (relating to proximal height) were recorded as a percentage of the height of the distal phalangeal bone in the horse, and as a percentage of the height of the proximal phalangeal bone in the elephant (digit III). For horse limbs, radiographs and external (palmar) pressure images were overlaid to identify x,y coordinates (relating to medio-lateral width and dorso-palmar length respectively (Fig. 6). Image J (1.45s/Java 1.6.0_20, National Institute of Health, USA) software was used to obtain the z coordinate. For elephant limbs, CT data were imported into Mimics software (v16.0, Materialise Ltd, Leuven, Belgium), where the needles and sole were reconstructed in 3D, before the model and the corresponding external (palmar) pressure image were overlaid to obtain x,y,z coordinates (Fig. 7). Mean external (palmar) pressures at the same x,y location as the needle tips were calculated from averaging the external pressures from the nine closest sensors over a period of 10 seconds (50 frames) at full load.

### Statistical Analysis

Linear mixed effect models (LMER, in R Programming Language (v.2.14.0); http://www.r-project.org/) were used to analyse the data. Although plotting load against pressure may have shown a quadratic relationship (due to digital cushion viscoelasticity), the addition of a quadratic term to the linear model did not make a significant contribution to model fit in either species. The quasi-static nature of load application was likely to negate any rate-dependant behaviour; therefore quadratic terms were omitted from the model:

Model = LMER(pressure ($Nm^{-2}$) ~ load (N) + (1 + load (N) | individual))

The fitted model included load (in Newtons, or as a % BW) as the fixed effect, and terms that allowed the intercept and linear term (slope) to vary by individual (Figs. S2-S5 show individual variation). To determine the significance of the fixed effect estimates, *P* values were generated, while comparisons between regions and comparisons between species were achieved using ANOVA and post hoc (Bonferroni) tests. Significance was set at $P<0.05$.

## Results

Individual forefeet were loaded a maximum of 20 times during the period of data collection; this provided four measures of internal pressure per load, per limb, totalling 339 observations in horse limbs (n = 7; see Fig. S2, S3 for individual variation) and 252 observations in elephant limbs (n = 6; see Fig. S4, S5 for individual variation). Replicating precise needle placement was difficult to achieve across individuals due to differences in foot size and conformation (Fig. 8 shows a relatively upright (A) versus flat-footed (B) conformation in two horses). Internal pressure data were therefore grouped by region; 1) deep central (d.c.), 2) superficial central (s.c.), 3) superficial medial (s.m.) and 4) superficial lateral (s.l.). Figure 9 shows normalised needle locations; i.e., as a percentage of foot width, length and distal phalangeal bone height in the horse or proximal phalangeal bone height in the elephant (digit III).

## Internal Pressure

The positive linear terms generated by the LMER analysis show that in both study taxa, and in all regions analysed, internal digital cushion pressure increased with load (Table 2). Excluding the deep central region in horse limbs, intercepts were not significantly different from zero. Mean and maximum instantaneous pressures in each region tended to follow a similar pattern. In horse limbs, increasing load had the greatest effect on pressures in the superficial central region (Fig. 10A). Conversely, in elephant limbs, increasing load had the least effect in the superficial central region (Fig. 10B). Our results revealed that horse limbs experienced higher starting magnitudes of pressure in the deep central region (i.e., both intercepts, for mean and maximum instantaneous pressure, were significantly different from zero, $P< 0.05$).

Of the four digital cushion locations analysed, some pressures differed depending on region (LMER, ANOVA, $P<0.05$, Tables 3 and 4). Post hoc analysis (Bonferroni) showed that in both species, central pressures were similar regardless of needle depth ($P>0.05$); furthermore, superficial central pressures differed from superficial medial pressures ($P<0.05$) in both species. Elephant digital cushion pressures were slightly more uniform (i.e., less variable) than horse digital cushion pressures.

Under equivalent loads (in terms of % BW), the superficial medial and lateral regions in elephant digital cushions experienced higher magnitudes of internal pressure when compared to medial and lateral regions in horse limbs (Fig. 11, ANOVA, $P<0.05$). Despite horse limbs experiencing higher starting magnitudes of pressure in the deep central regions of the digital cushion, increasing load had a similar effect on central pressures in both species (ANOVA, $P>0.05$).

## External pressure (at the palmar surface)

Substantial technical issues with the pressure pad arose during data collection (see Data S9 for details), and the plate was sent back to the manufacturer for repair. The data reported here are for 5 horse and 5 elephant forelimbs. Figs. S7 and S8 show that foot placement generated CoPs that were central to the feet, as per the observations during data collection. The pressure pad is optimised for (clinical) human use, i.e., a 70 kg person loading the pad to ~ 1-2 times BW during activity. As the maximum capacity of the pressure pad was 200 $Ncm^{-2}$, pressure values above this threshold were disregarded as unreliable. The remaining external pressures that we measured have the same order of magnitude as previously reported values (Table 5); at standing forelimb loads (~30 % BW), mean external palmar foot pressure was higher in horse feet compared to elephant feet (although there were insufficient data to test this statistically).

The palmar surface area (SA) in elephant forefeet was around seven times larger than the palmar SA of horse forefeet (Table 6), whereas elephant body masses were around six times larger (Table 1). At the level of the needle tips (i.e., where internal pressure was sampled), the digital cushion's cross-sectional area (CSA) constituted one-fifth and one-third of the total palmar foot SA in horses and elephants respectively.

There was only a weak correlation between applied load and external palmar pressure ($r$=0.36 and $r$=0.31 in horses and elephants respectively); the distribution of pressures over the palmar surface was more variable in elephant forefeet (Table 6). Internal digital cushion pressures were consistently higher than external palmar pressures in the same (x,y) location (Mann Whitney U Test, $P$<0.05), and there was minimal correlation between internal and external pressure ($r$<0.25).

## Discussion

We aimed to characterise loads inside and outside the forefeet of horses and elephants in order to compare the influence of extreme digital cushion (and foot) morphology on pressure magnitudes and distributions. Our results reveal that (*ex vivo*) axial limb loading causes internal digital cushion pressure to increase, and regional pressure differences exist within the digital cushion. Further, under equivalent loads (in terms of % BW), elephant feet experience higher medial and lateral pressures than horse feet do.

Previous studies have inferred that the lateral portion of the elephant manus experiences greater palmar pressures (Panagiotopoulou *et al.,* 2012) and perhaps bone or tendon stresses (Miller *et al.,* 2008). Yet we find that the highest internal pressures are located in the medial (and then lateral) regions of the digital cushion. It is conceivable that the *ex vivo* loading set-up or limb conformation abnormalities induced asymmetrical loading at the level of the foot (Luikart and Stover 2005). However, this would have been reflected in the location of the CoPs (Figs. S7 and S8 show CoPs were consistently central). As a potential explanation for these results, we speculate that high medial pressures are caused by the prepollex (see Hutchinson *et al.,* 2011) directly transferring load to the digital cushion.

Internal chamber geometry and distribution remains undetermined in elephant digital cushions. In human heel pads, the presence of chambers is associated with preventing bulk flow and gross distortion (Ker 1999); this additional information could help to explain digital cushion behaviour in elephant limbs under load. On the basis of the variation in digital cushion pressure shown here, we propose that material properties differ throughout the digital cushion due to differences in structural organisation. The medial (and perhaps lateral-) portions of the digital cushion in elephants experience higher pressures; this may be due to greater fibrous tissue content and/or smaller chambers (Hsu *et al.,* 2007). This would also fit with the observation that their feet land with a slightly lateral CoP trajectory (Panagiotopoulou *et al.,* 2012). The expectation that pressure in the deep central digital cushion region remains more stable until large loads are applied was not fulfilled; although the assumption that this expectation was based on is likely to be correct (macro-chambers have greater initial compliance in human heel pads, Hsu *et al.,* 2007). MRI-guided needle insertion would be required to confirm needle placement within specific chambers to investigate this further.

In contrast to elephants, in horse forefeet we found that the highest internal pressures are located in the superficial central region. This may be accounted for by the large degree of extension in the DIP joint, causing the middle phalangeal bone to compress this region of the digital cushion (Taylor *et al.,* 2005). Although increasing load has less effect on pressure in the deep central region, we speculate that the higher starting magnitudes of pressure are due to this portion being thinner, denser and more rigidly contained on all aspects. We acknowledge that the locations sampled for pressures in horse and elephant forefeet are not strictly homologous, but both taxa are so radically transformed and insertion of needles into precise locations is so difficult that strict application of topological homology in our experimental setup was not practical.

Pressures within the digital cushion were higher in magnitude than the external palmar pressures, consistent with previous finite element models of human heel pads (Spears *et al.,* 2007; Luo *et al.,* 2011). The absence of a stronger (linear) correlation between external and internal pressure in the same (x,y) location is not surprising, because previous studies have suggested external forces

are poor indicators of internal stresses (Loerakker 2007). In contrast to the negative allometry of plantar foot SA that Michilsens *et al.,* (2009) reported, we found that palmar foot SA in elephant feet increases to a greater extent than body mass. This explains our finding that (mean) palmar pressures were lower in magnitude in elephant feet compared to horse feet. The ratio of palmar foot SA to contact area was 45% greater in horses, supporting the inference that elephants use a greater proportion of the foot's available SA to support load, which could help protect their sole from high pressures. It remains unclear how the concavity of a horse's sole benefits the animal (although this feature appears to be highly variable; Fig. 8); certainly, limiting the contact area is counter-productive to reducing pressure. It is likely that the concavity aids friction and grip (Pardoe *et al*., 2001), allowing horses to move at faster speeds on loose or soft surfaces, and the reduction of tissue volume it provides surely keeps foot mass low, with consequent energetic benefits for swinging the distal limb (Wilson and Weller 2011).

From prior studies (Weissengruber *et al.,* 2006; Egerbacher *et al.,* 2005), it seems likely that the semi-fluid material inside elephant digital cushions would "flow" more easily than the material inside horse digital cushions due to the higher adipose tissue content present in elephant digital cushions. Yet it is unclear how fat content influences digital cushion function; Buschmann *et al.,* (1993) suggested that lower viscosity associated with adipose tissue enhances efficiency of the human heel pad (although they were focused on shock absorption). Bowker (2003), on the other hand, associated adipose tissue with sub-optimal foot function in horses (although again, the focus was on shock absorption). In our study, higher adipose content (in elephant digital cushions) is associated with higher internal pressures (medial and lateral digital cushion regions only).

Although quantifying pressure in four regions gives an incomplete description of the internal stress state throughout the cushion, the use of more needles was considered too damaging to the structure and not feasible in the time frame of the study. The capacity of the force platform (~24,000 N) prevented elephant limbs from being loaded to a similar extent as horse limbs; maximal loads in elephant limbs were only 50-60% BW, whereas maximal loads in horse limbs represented >150% BW. The pressure pad was also operating at near-maximum capacity (200 $Ncm^{-2}$), and despite correcting the pad's force measurements (using the force platform), much of the external pressure data had to be excluded from the analysis (as reported in the Results section and detailed in Data S9). The *ex vivo* magnitudes of palmar foot pressure are comparable to *in vivo* values previously reported (Panagiotopoulou *et al.,* 2012); however, it is surprising that increasing load did not have a stronger linear correlation with external pressure magnitudes. This anomaly can best be ascribed to the pad being optimised for human use (i.e., at much lower loads).

Rate of loading is an important consideration in this study, because viscoelastic tissues have non-linear and rate-dependant responses to loading (Ker 1999; Hsu *et al.,* 2007). The manually operated hydraulic ram could not replicate high physiological loading rates. Although some analysis of the digital cushion's viscoelastic response could have been included, its biological relevance would have been questionable, because loading rate (via the ram) was so slow. Applying rapid and large loads (~30 kN for 0.30 second stance time in a fast-moving elephant, Hutchinson *et al.,* 2006) was not feasible with the equipment available and was deemed unsafe. The fixed point application of load differs from physiological loading whereby a dynamic pattern exists; during *in vivo* locomotion, the point of application starts at the posterior of the foot and moves cranially throughout the stance phase (Panagiotopoulou *et al*., 2012; van Heel *et al*.,

2005). This study's purpose was largely comparative and hence a static approach (replicating standing and mid-stance) was judged to be sufficient as well as the most practical option.

Although elephant limbs were loaded at a slightly faster rate than horse limbs, previous work has shown that *in vivo* loading rates in elephants exceed those in horses (~17,000 $Ns^{-1}$ and ~7000 $Ns^{-1}$ in elephants and horses respectively at relatively comparable walking speeds; Warner *et al.,* 2013). Ker (1996) found slight creep in human heel pads under *ex vivo* test conditions (1.4 kN, using continuous sinusoidal applications of force); however, it was concluded that this creep was reversible and not associated with tissue damage. We assume that digital cushion deformation as a result of loading did not become permanent (causing internal pressures to remain high, Aerts *et al.,* 1995; Ker 1996), because post-load pressures returned to pre-loading magnitudes.

Although freezing is unlikely to alter the mechanical properties of human heel pads (Bennett and Ker 1990a; Ker 1996), the thawing process and data collection period (at room temperature) could have resulted in some tissue dehydration. Despite moisture levels being known to affect material properties (Bertram and Gosline 1987; Douglas *et al.,* 1996), it was not feasible to monitor or account for dehydration. Limb deformation may have been reduced as a result of increased tissue stiffness (via dehydration) but using fresh specimens was unrealistic, especially with regards to elephant limbs. Furthermore, absolute measurements of *in vivo* stiffness were not our target; thus for comparative purposes the data should be reasonable approximations.

There have been no prior internal pressure measurements for elephant feet, and only one in horses (*in vivo*) (Dyhre-Poulsen *et al.,* 1994). Although it is reasonable to expect some differences between *ex vivo* and *in vivo* limb loading studies (because active and haemodynamic mechanisms associated with force attenuation are absent and tissue properties may change post-mortem; Riemersma 1996), our study is nevertheless valuable, providing insight into how internal digital cushion stresses change in response to load. It is interesting to note that in human medicine, pressures of ~ 4000 $Nm^{-2}$ require surgical decompression (Wall *et al.,* 2010; Rasul 2011); although digital cushion tissue differs from muscle tissue, the internal digital cushion pressures reported here are almost two times as high.

Elephant pressures are slightly more uniform throughout the digital cushion; however, describing the digital cushion as acting as a fluid-filled sac is inappropriate, because pressure is not equal in all locations (i.e., Pascal's theory does not apply). We speculate that the variation in pressure throughout the digital cushion is likely to be due to heterogeneities in material properties and/or structural organisation causing differential deformation. Further work will focus on quantifying the effect of load on 3D digital cushion deformation to test the latter speculation. Internal pressure magnitudes exceed external palmar foot magnitudes, matching the predictions of previous finite element studies (Spears *et al.,* 2007; Luo *et al.,* 2011).

## Conclusion

Insufficient functional capacity in human heel pads can lead to the development of shock-induced discomfort and injury (Kinoshita *et al.,* 1996). If high pressures can induce pathology (e.g. Panagiotopoulou *et al.,* 2012), based on the magnitudes measured in this study, we propose that the medial (and lateral) bony prominences in elephant feet may be vulnerable. Indeed, two recent studies of rhinoceroses indicated that osteopathologies are more prevalent in the medial digit (Galanteanu *et al.,* 2013; Regnault *et al*., 2013). If large variation in pressures (indicating poor pressure distribution) induces pathology, based on the variation in pressure measured in this

study, we propose that the elephant's external palmar tissues and the horse's internal (digital cushion) tissues may be susceptible to pressure-related pathology. Determining how the digital cushion responds to loading *ex vivo* may highlight potential weaknesses within the foot and assist our understanding of why mechanically induced pathologies develop.

## List of Abbreviations

| | |
|---|---|
| BW | body weight |
| CoP | centre of pressure |
| CSA | cross-sectional area |
| CT | computed tomography |
| d.c. | deep central |
| LMER | linear mixed effect model (in R software) |
| MRI | magnetic resonance imaging |
| SA | surface area |
| s.c. | superficial central |
| s.l. | superficial lateral |
| s.m. | superficial medial |


## Acknowledgements

We thank Yu Mei Chang (RVC Statistician) for advice on LMER analysis, numerous EU zoos/safari parks for provision of elephant cadaver material, Holts Abattoir for supplying horse cadavers and Paul Foster at Southwest Medical Ltd for loaning us the Datex Ohmeda equipment used in this study. In addition, we thank Luis Lamas, Joanne Gordon and the staff of the RVC Imaging Suite for the CT scans and radiographs. Finally we thank Chris Seymour, Jeff Rankin, James Usherwood, Simon Wilshin, Chris Pardoe, Pete Day and Renate Weller for useful discussions, along with other members of the Structure & Motion Lab.


## References


Aerts, P., Kerr. R. F., De Clercq. D. and Ilsley. D.W. 1996. The effects of isolation on the mechanics of the human heel pad. *Journal of Anatomy*. 188:417-423.

Alcantara. E., Forner. A., Ferrus. E., Garcia. A. and Ramiro. J. 2002. Influence of age, gender, and obesity on the mechanical properties of the heel pad under walking impact conditions. *Journal of Applied Biomechanics*. 18(4): 345.

Alexander. R. M., Bennett. M. and Ker. R. 1986. Mechanical properties and function of the paw pads of some mammals. *Journal of Zoology*. 209:405-419.

Back. W., Schamhardt. H.C., Hartman. W. and Barneveld. A. 1995. Kinematic differences between the distal portions of the forelimbs and hindlimbs of horses at the trot. *American Journal of Veterinary Research*. 56(11):1522-1528.

Bertram. J. E and Gosline. J. M. 1987. Functional design of horse hoof keratin: the modulation of mechanical properties through hydration effects. *Journal of Experimental Biology*. 130:121-136.

Bowker. R. M. 2003. Contrasting structural morphologies of 'good' and 'bad' footed horses. Proceedings: 49th Annual Convention of the American Association of Equine Practitioners, 2003, New Orleans, Louisiana, (Ed.).

Buschmann. W. R., Hudgins. L. C., Kummer. F., Desai. P. and Jahss. M. H. 1993. Fatty acid composition of normal and atrophied heel fat pad. *Foot Ankle*. 14(7):389-94.

Chi. K. J. and Roth. V. L. 2010. Scaling and mechanics of carnivoran footpads reveal the principles of footpad design. *Journal of the Royal Society Interface*. February 24, 2010 doi:10.1098/rsif.2009.0556

Crevier-Denoix. N., Robin. D., Pourcelot. P., Falala. S., Holden. L., Estoup. P., Dequilbet. L., Denoix. J.-M. and Chateau. H. 2010. Ground reaction force and kinematic analysis of limb loading on two different beach sand tracks in harness trotters. *Equine Veterinary Journal Supplement.* 38:544-51.

De Clercq. D., Aerts. P. and Kunnen. M. 1994. The mechanical characteristics of the human heel pad during foot strike in running: an in vivo cineradiographic study. *Journal of Biomechanics*. 27(10):1213-22.

Douglas. J. E., Biddick. T. L., Thomasson. J. J. and Jofriet. J. C. 1998. Stress/stain behaviour of the equine laminar junction. *Journal of Experimental Biology*. 201:2287-2297.

Douglas. J. E., Mittal. C., Thomasson. J. J. and Jofriet. J. C. 1996. The modulus of elasticity in the equine hoof wall: implications for the mechanical function of the hoof. *Journal of Experimental Biology*. 199:1829–1836.

Dyhre-Poulsen. P., Smedegaard. H. H., Roed. J. and Korsgaard. E. 1994. Equine hoof function investigated by pressure transducers inside the hoof and accelerometers mounted on the first phalanx. *Equine Veterinary Journal*. 26(5):362-366.

Egerbacher. M., Helmreich. M., Probst. A., Konig. H. and Bock. P. 2005. Digital cushion in horses comprise coarse connective tissue, myxoid tissue and cartilage but only uniocular fat tissue. *Anatomia, Histologia, Embryologia*. 34(2):112-116.

Hutchinson, J. R. 2009. Response: Of ideas, dichotomies, methods, and data – how much do elephant kinematics differ from those of other large animals? *Journal of Experimental Biology*. 212:153-154.

Hsu. C. C., Tsai. W. C., Wang. C. L., Pao. S. H., Shau. Y. W. and Chuan. Y.S. 2007. Microchambers and macrochambers in heel pads: are they functionally different? *Journal of Applied Physiology*. 102:2227-2231.

Jayes. A. S., Alexander. R. McN. 1978 Mechanics of locomotion of dogs (*Canis familiaris*) and sheep (*Ovis aries*). *Journal of Zoology*. 185:289-308.

Ker. R. F. 1996. The time-dependent mechanical properties of the human heel pad in the context of locomotion. *Journal of Experimental Biology*. 199(7):1501-1508.

Ker. R. F. 1999. The design of soft collagenous load-bearing tissues. *Journal of Experimental Biology*. 102(23):1315-1324.

Loerakker. S. 2007. Aetiology of pressure ulcers. D. Phil. Thesis, Eindhoven University of Technology.

Luikart. K. A. and Stover. S. M. 2005. Chronic ulcerations associated with degenerative bone disease in two Asian elephants (Elephas Maxmimus). *Journal of Zoo Wildlife Medicine*. 36(4):684-688.

Luo. G, Houston. V. L., Garbarini. M. A., Beattie. A. C., Thongpop. C. 2011. Finite element analysis of heel pad with insoles. *Journal of Biomechanics*. 44(8):1559-65.
Manter. J. T. 1938. The dynamics of quadrupedal walking. *Journal of Experimental Biology*. 15:522-540.
McGuigan. P. and Wilson. A. M. 2003. The effect of gait and digital flexor muscle activation on limb compliance in the forelimb of the horse *Equus caballus*. *Journal of Experimental Biology.* 206(8):1325-36.
Michelsens. F., Aerts. P., Van Damme. R. and D'Aout. K. 2009. Scaling of plantar pressure in mammals. *Journal of Zoology*. 279:236-242.
Miller. C. M., Basu. C., Fritsch. G., Hildebrandt. T. and Hutchinson. J. R. 2008. Ontogenetic scaling of foot musculoskeletal anatomy in elephants. *Journal of the Royal Society Interface*. 5:465-476.
Mueller. M. J. and Maluf. K. S. 2002. Tissue adaptation to physical stress: a proposed "physical stress theory" to guide physical therapist practice, education and research. *Journal of the American Physical Therapy Association*. 82:383-403.
Oosterlinck. M., Pille. F., Back. W., Dewulf. J., Gasthuys. F. 2011. A pressure plate study on fore and hindlimb loading and the association with hoof contact area in sound ponies at the walk and trot. *The Veterinary Journal*. 190:71-6.
Panagiotopoulou. O., Pataky. T. C., Hill. Z. and Hutchinson. J. R. 2012. Statistical parametric mapping of the regional distribution and ontogenetic scaling of foot pressures during walking in Asian elephants (Elephas maximus). *Journal of Experimental Biology*. 215:1584-1593.
Pardoe. C. H., McGuigan. M. P., Rogers. K. M., Rowe. L. L., Wilson. A. M. 2001. The effect of shoe material on the kinetics and kinematics of foot slip at impact on concrete. *Equine Veterinary Journal Supplement*. 33: 70-73.
Raber. M., Lischer. C., Geyer. H. and Ossent. P. 2004. The bovine digital cushion - a descriptive anatomical study. *The Veterinary Journal*. 167:258-264.
Rasul. A. T. 2011. Acute Compartment Syndrome. Medscape Reference. http://emedicine.medscape.com/article/307668-overview (Accessed June 2012).
Regnault. S., Hermes. R., Hildebrandt. T., Hutchinson. J. R., Weller. R. 2013. Osteopathology in the feet of Rhinoceroses; lesion type and distribution. *Journal of Zoo and Wildlife Medicine*. 44(4):918-927.
Ren. L., Butler. M., Miller. C., Paxton. H., Schwerda. D., Fischer. M. S. and Hutchinson. J. R. 2008. The movements of limb segments and joints during locomotion in African and Asian elephants. *Journal of Experimental Biology*. 211:2735-2751.
Ren. L., Miller. C., Lair. R. and Hutchinson. J. R. 2010. Integration of biomechanical compliance, leverage, and power in elephant limbs. *Proceedings of the Natural Academy of Science*. 107:7078-7082.
Riemersma. D. J., van den Bogert. A. J., Jansen. M. O. and Schamardt. H. C. 1996. Tendon strain in the forelimbs as a function of gait and ground characteristics and in vitro limb loading in ponies. *Equine Veterinary Journal*. 28(2):133-138.
Spears. I. R., Miller-Young. J. E., Sharma. J., Ker. R.F. and Smith. F.W. 2007. The potential influence of the heel counter on internal stress during static standing: a combined finite element and positional MRI investigation. *Journal of Biomechanics*. 40(12):2774-2780.
Spears. I. R., Miller-Young. J. E., Waters. M. and Rome. K. 2005. The effect of loading conditions on stress in the barefooted heel pad. *Medicine and Science in Sports Exercise*. 37(6):1030-1036.
Taylor. D. D., Hood. D. M., Potter. G. D., Hogan. H. A. and Honnas. C. M. 2005. Evaluation of displacement of the digital cushion in response to vertical loading in equine forelimbs. *American Journal of Veterinary Research*. 66(4):623-630.

553 Thomason. J. J., Biewener. A. A. and Bertram. J. E. A. 1992. Surface strain on the equine hoof
554 wall in vivo: implications for the material design and functional morphology of the wall. *Journal*
555 *of Experimental Biology*. 166:145-168.
556 van Heel. M. C. V., Moleman. M., Barneveld. A., van Weeren. P. R., Back. W. 2005. Changes in
557 location of centre of pressure and hoof-unrollment pattern in relation to an 8-week shoeing
558 interval in the horse. *Equine Veterinary Journal*. 37(6):536-540.
559 Wall. C. J., Lynch., J. Harris. I. A., Richardson. M. D., Brand. C., Lowe. A. J. and Sugrue. M.
560 2010. Clinical practice guidelines for the management of acute limb compartment syndrome
561 following trauma. *ANZ J. Surgery*. 80(3):151-156.
562 Warner. S. E. 2014. Foot design, locomotor impact mechanics and pathology in large mammals.
563 D. Phil. Thesis, The Royal Veterinary College, UK.
564 Warner. S. E., Pickering. P., Panagiotopoulou. O., Pfau. T., Ren. L., Hutchinson. J. R. 2013. Size-
565 related changes in foot impact mechanics in hoofed mammals. *Plos One*. 8(1):e54784.
566 Weissengruber, G. E., Egger, G. F., Hutchinson, J. R., Groenewald, H. B., Elsasser L., Famini. D.
567 and Forstenpointner. G. 2006. The structure of the cushions in the feet of African elephants
568 (Loxodonta africana). *Journal of Anatomy*. 209:781-792.
569 Wilson. A. M., Weller. R. (Chapter 26) In Ross. M. W. and Dyson. S. J. (2011). Diagnosis and
570 management of lameness in the horse. 2nd Ed, Elsevier Saunders, Missouri, USA.

# Figure 1

Schematic diagram of foot posture in horses and elephants.

Horses are unguligrades (A); the most distal phalangeal bone supports body weight via the hoof (Douglas *et al.,* 1998; Bowker 2003); the carpal (or tarsal) bones, metapodials and phalanges are permanently raised off the ground. In contrast, elephants have a sub-unguligrade foot posture (B), however their digital cushion renders them functionally plantigrade, because the digital cushion (containing an enlarged strutlike “predigit”) directly supports body weight (Miller *et al.,* 2008; Hutchinson *et al.,* 2011).

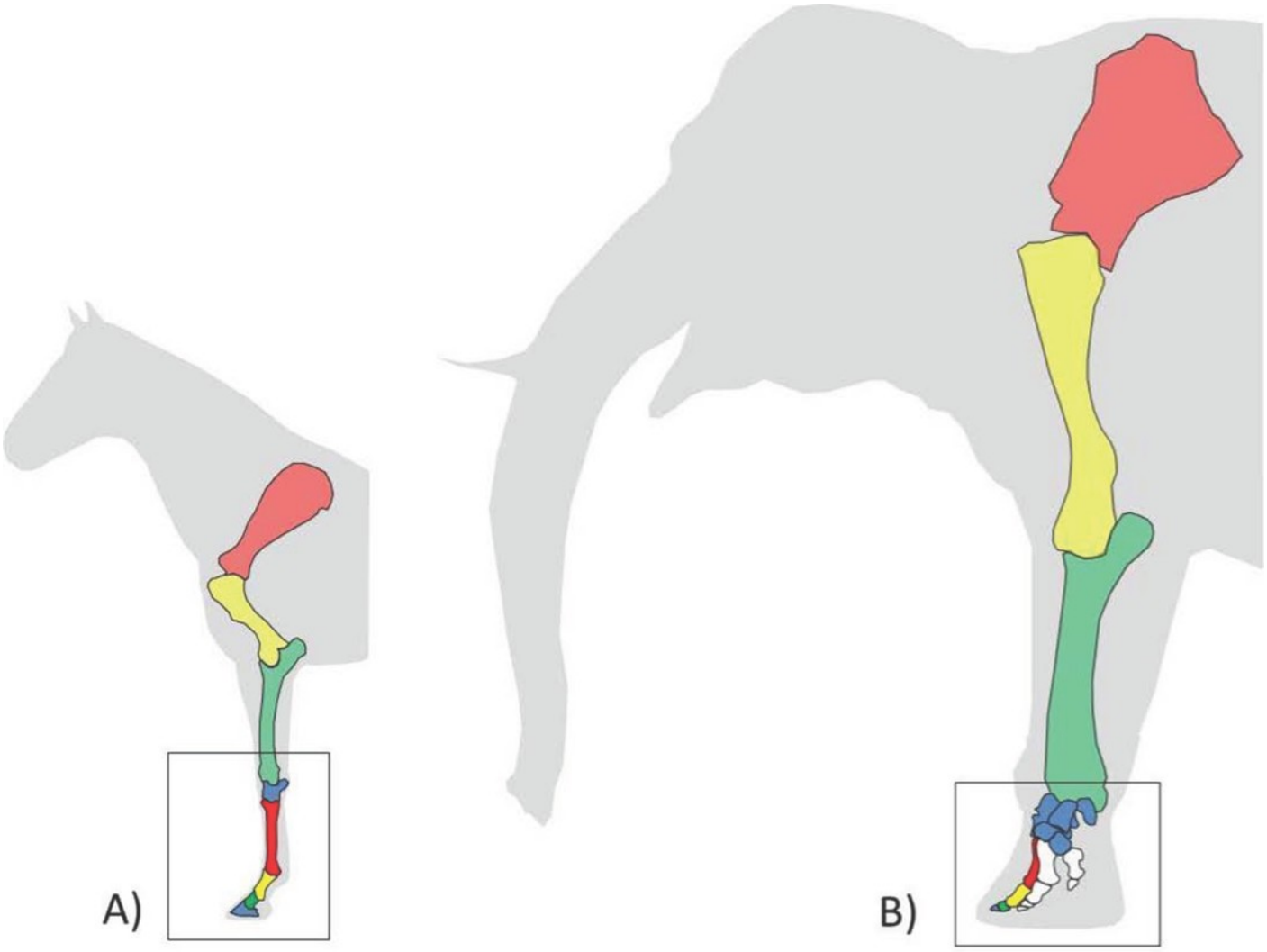




*PeerJ PrePrints* | http://dx.doi.org/10.7287/peerj.preprints.231v1 | CC-BY 4.0 Open Access | received: 2 Feb 2014, published: 2 Feb 2014

# Figure 2

High resolution MR images of horse (A) and elephant (B) digital cushions (sagittal cross sections).

Digital cushions are outlined in red; compartments are outlined in white. No compartments can be visually detected in horse digital cushions, whereas it appears the smaller (micro) chambers are located more superficially than the larger (macro) chambers in elephant digital cushions.

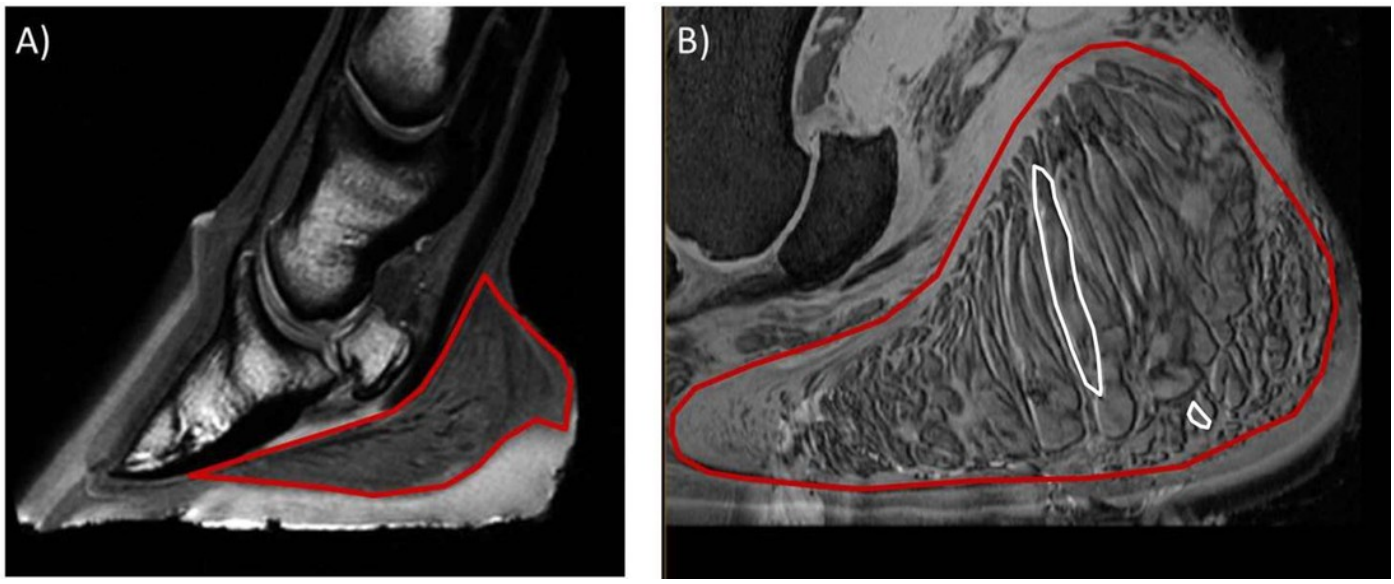




*PeerJ PrePrints* | http://dx.doi.org/10.7287/peerj.preprints.231v1 | CC-BY 4.0 Open Access | received: 2 Feb 2014, published: 2 Feb 2014

# Figure 3

Internal pressure sampling (needle) locations in horse digital cushions.

A) Sagittal MR section showing intended sampling locations within the digital cushion (pink), Red shows the deep central location, blue shows the superficial central, yellow shows the superficial medial and green shows the superficial lateral location. B) Lateral radiograph with needles *in situ*. C) coronal MR section showing intended sampling locations within the digital cushion. D) dorsal-palmar radiograph with needles *in situ*.

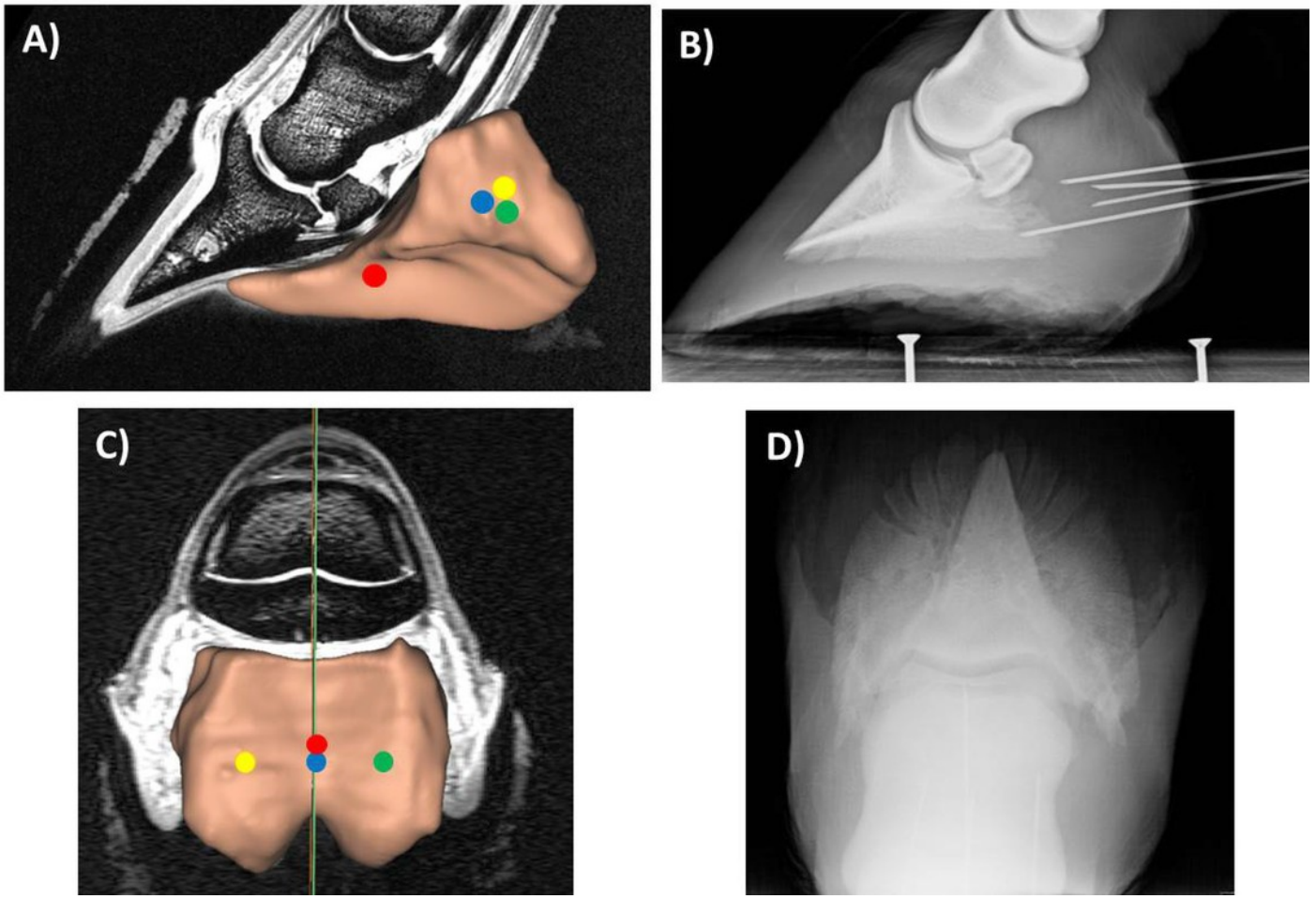




*PeerJ PrePrints* | http://dx.doi.org/10.7287/peerj.preprints.231v1 | CC-BY 4.0 Open Access | received: 2 Feb 2014, published: 2 Feb 2014

# Figure 4

Internal pressure sampling (needle) locations in elephant digital cushions.

A) Sagittal MR section showing intended sampling locations within the digital cushion (pink), Red shows the deep central location, blue shows the superficial central, yellow shows the superficial medial and green shows the superficial lateral location. B) Sagittal CT section with needles *in situ* (only the deep central needle is visible). C) coronal MR section showing intended sampling locations within the digital cushion. D) Axial CT section with needles *in situ* (needle tips are shown in turquoise).



*PeerJ PrePrints* | http://dx.doi.org/10.7287/peerj.preprints.231v1 | CC-BY 4.0 Open Access | received: 2 Feb 2014, published: 2 Feb 2014

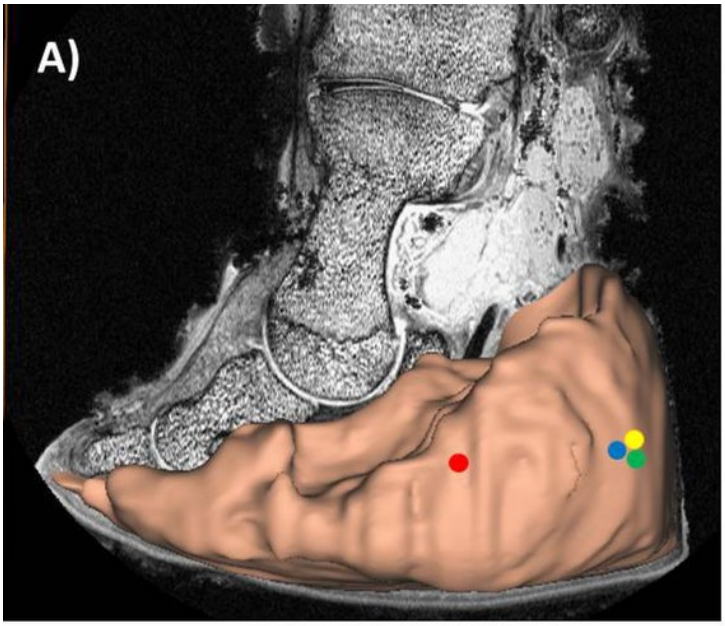



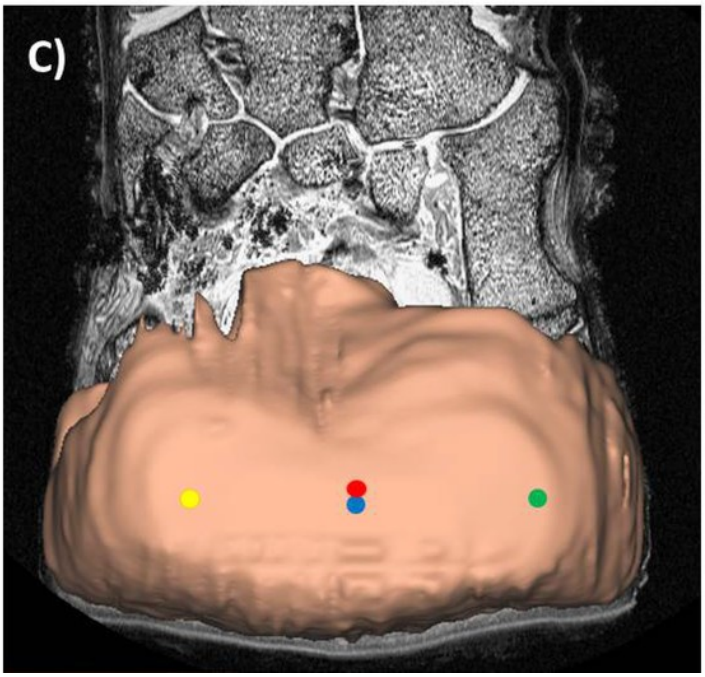


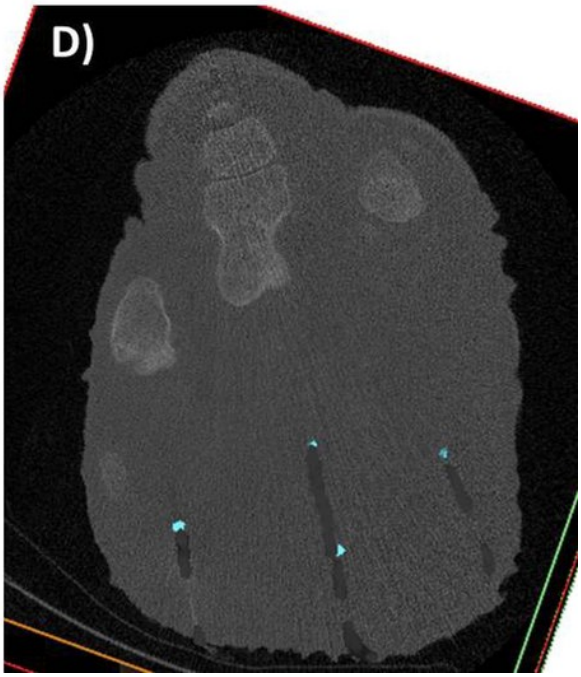




*PeerJ PrePrints* | http://dx.doi.org/10.7287/peerj.preprints.231v1 | CC-BY 4.0 Open Access | received: 2 Feb 2014, published: 2 Feb 2014

# Figure 5

Data output from a 12 minute trial (horse limb loaded to 112 % body weight).

A) Pressure (mmHg) from the four transducers measuring internal digital cushion (DC) pressure and B) applied force (kN) from the Kistler force plate. Data were averaged over a 30 second window (grey shaded areas); the change in internal pressure was calculated by subtracting the average pressure under no load, from the average pressure under load to give mean internal pressure as a result of load. Maximum instantaneous pressure was also recorded (i.e., the maximum pressure change following load application) as was the rate of force application.

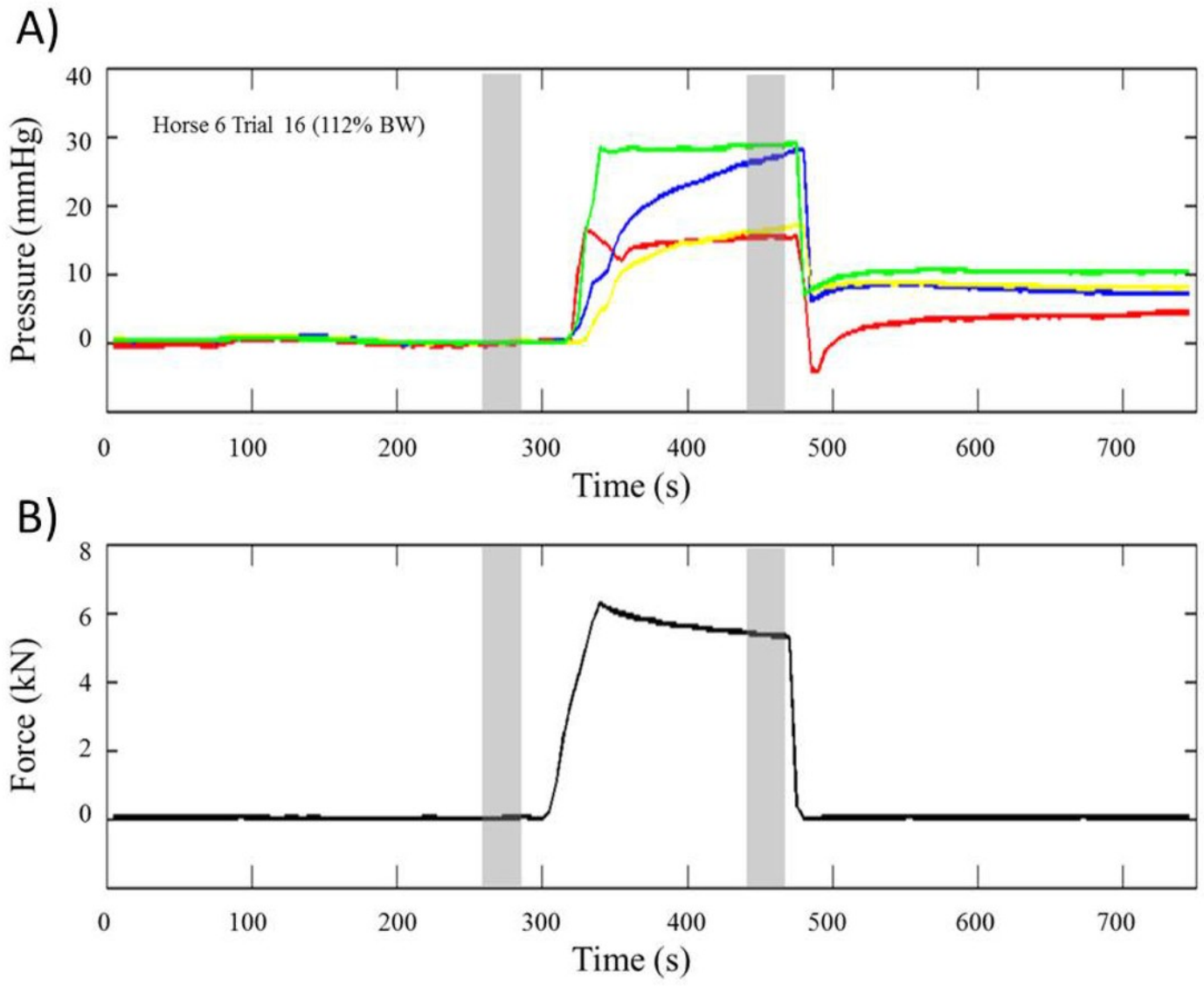




*PeerJ PrePrints* | http://dx.doi.org/10.7287/peerj.preprints.231v1 | CC-BY 4.0 Open Access | received: 2 Feb 2014, published: 2 Feb 2014

# Figure 6

Method to determine x,y location of needle tips within the horse digital cushion.

Using dorso-palmar (A) and medio-lateral radiographs (B), the needle tips could be expressed as a percentage of foot width (x) and length (y). This information (i.e., the coordinates) was transposed onto the external pressure maps (C and D), to identify the location of the nine pressure pad sensors closest to the x,y needle tip. External pressures were calculated by averaging pressure across these nine sensors. Warm colours in C denote higher pressures, whereas cool colours denote lower pressures, black areas show zero pressure. Red is for the deep central, blue is for the superficial central, yellow is for the superficial medial and green is for the superficial lateral needle location, shown by the colour coded crosses.

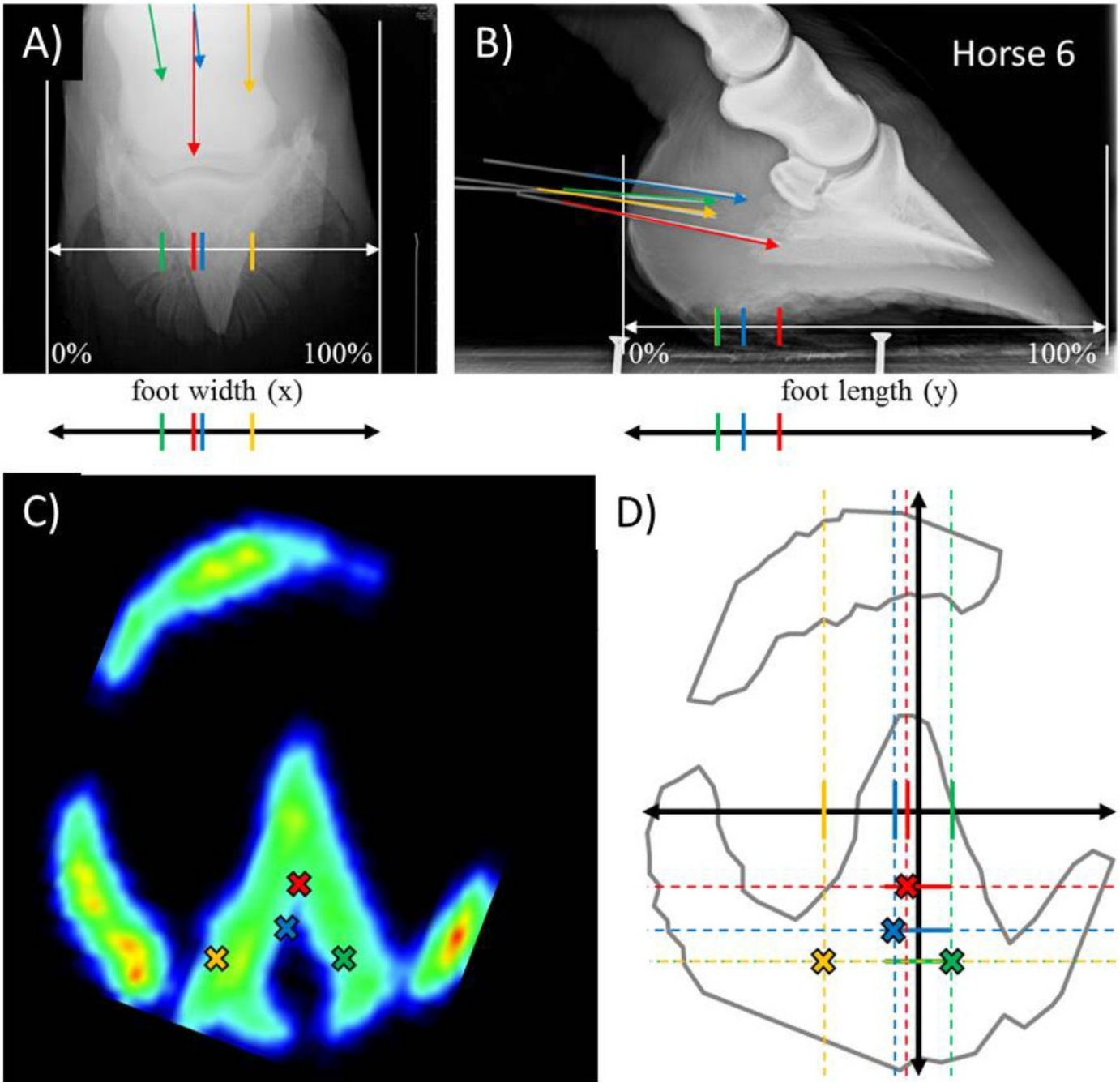

# Figure 7

Method to determine x,y location of needle tips within the elephant digital cushion. <!--? R&#65533;

Using reconstructed three dimensional (3D) models from computer tomography (CT) data (A and B), the location of each needle tip could be expressed as a percentage of foot width (x) and length (y). This information was transposed onto the external pressure maps (C and D), to identify the location of the nine pressure pad sensors closest to the x,y needle tip. External pressures were calculated by averaging pressure across these nine sensors. Warm colours in C denote higher pressures, whereas cool colours denote lower pressures, black areas show zero pressure. Red is for the deep central, blue is for the superficial central, yellow is for the superficial medial and green is for the superficial lateral needle location, shown by the colour coded crosses.

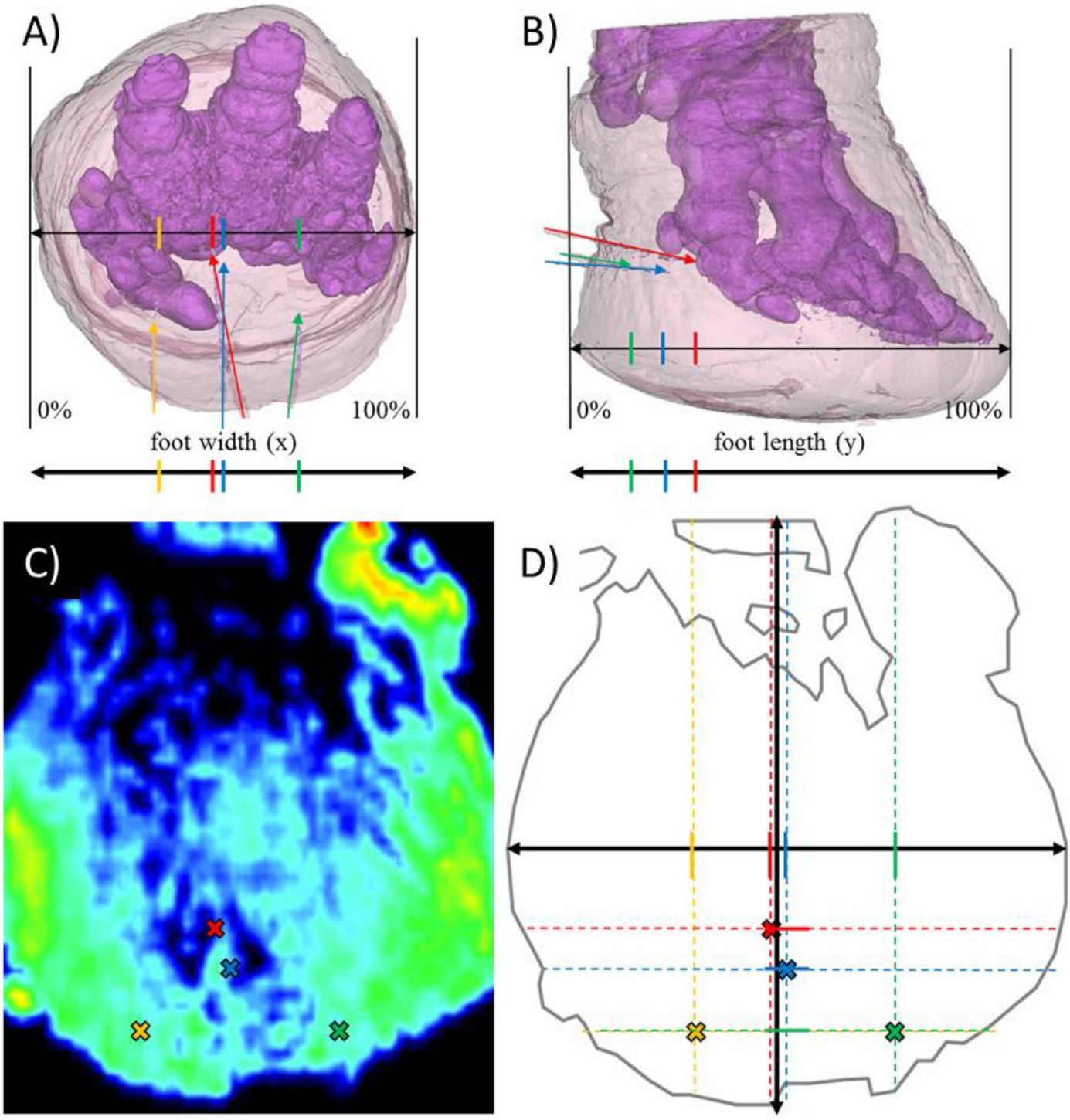

# Figure 8

Radiographs showing variation in (horse) foot conformation.

Needle placement was difficult to replicate across individuals based on external foot landmarks.

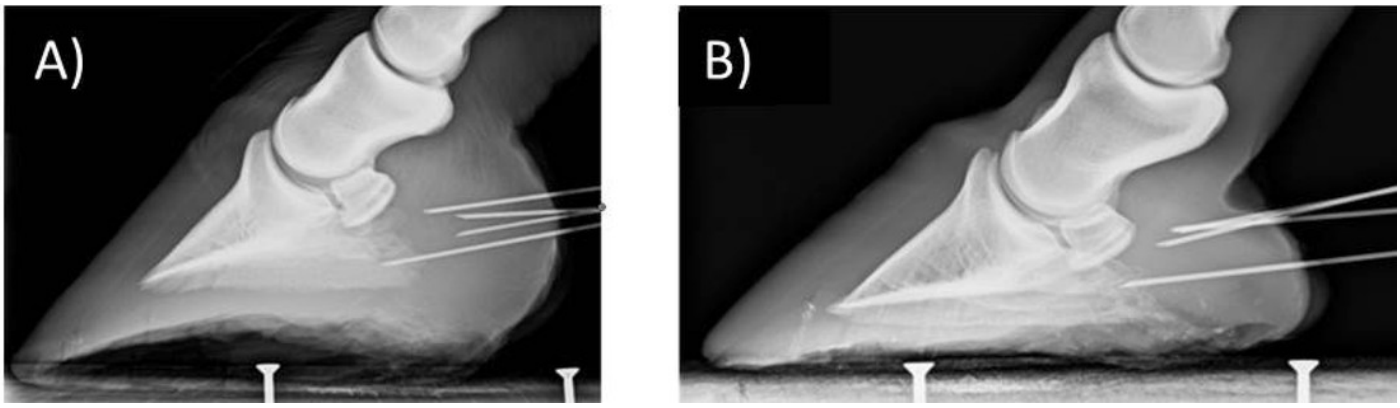




*PeerJ PrePrints* | http://dx.doi.org/10.7287/peerj.preprints.231v1 | CC-BY 4.0 Open Access | received: 2 Feb 2014, published: 2 Feb 2014

# Figure 9

Normalised needle tip locations (as a % of foot width, foot length and proximal or distal phalanx height.

A) Lateral view of horse foot, B) lateral view of an elephant foot, C) palmar view of horse foot, D) palmar view of an elephant foot. Colour coded filled circles show where pressures in each region were sampled; red is for deep central, blue is for superficial central, yellow is for superficial medial and green is for superficial lateral pressures.

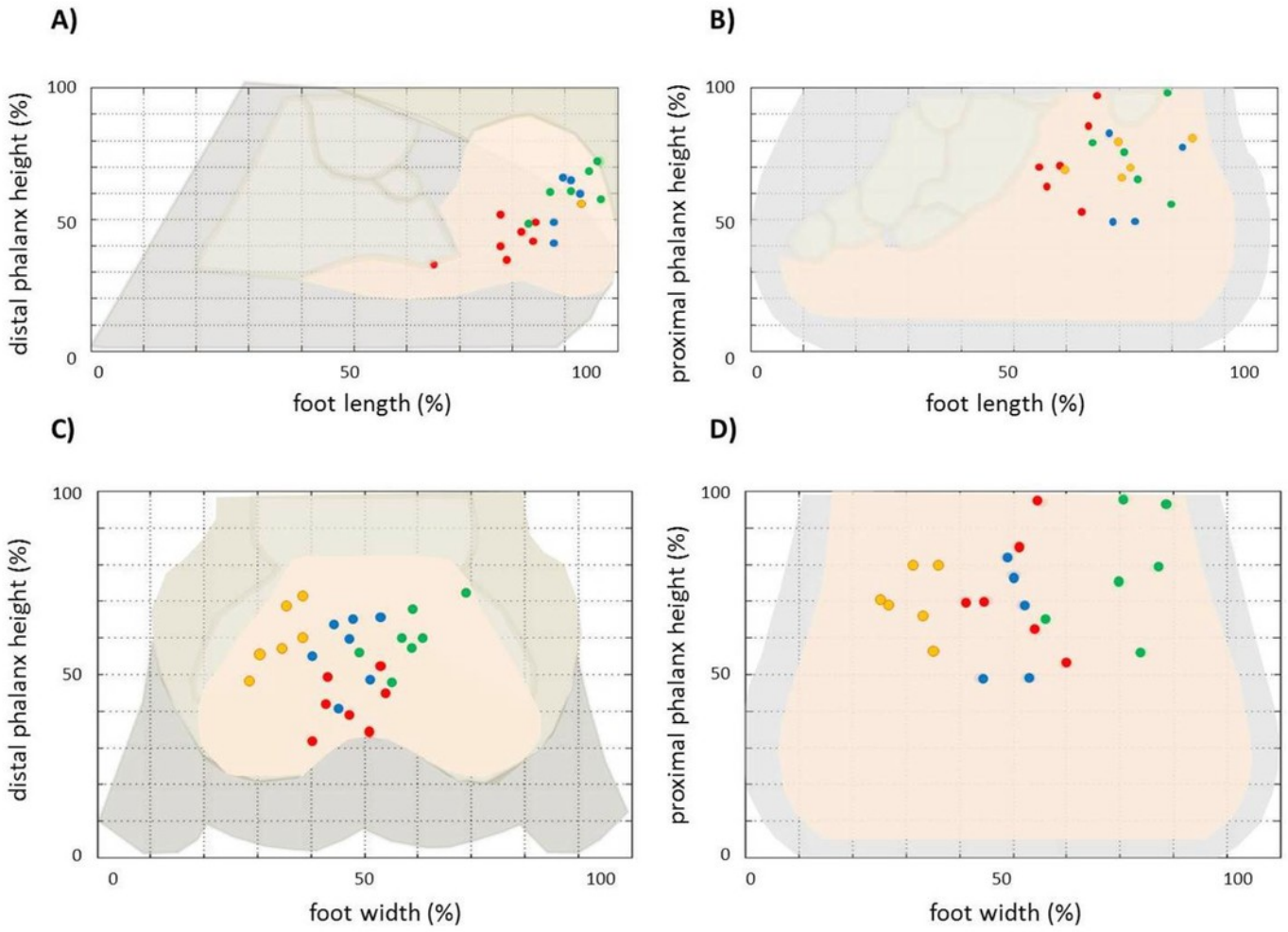




*PeerJ PrePrints* | http://dx.doi.org/10.7287/peerj.preprints.231v1 | CC-BY 4.0 Open Access | received: 2 Feb 2014, published: 2 Feb 2014

# Figure 10

LMER Results: Mean internal pressure in each digital cushion (DC) location for A) horses and B) elephants.

Mean internal pressure ($Nm^{-2}$) is plotted against the applied force (N, from the force platform). Colour coded markers show pressure magnitudes in each region; red circles are for deep central, blue triangles are for superficial central, yellow diagonal crosses are for superficial medial and green vertical crosses are for superficial lateral pressures. N.B. the x axis is different between plots, 0-7000 N in horses represents loads of 0-150 % body weight (BW) (A), whereas 0-30,000 N in elephants represents loads of 0-60 % BW (B). Applying larger loads would have exceeded the force platform's maximal capacity.

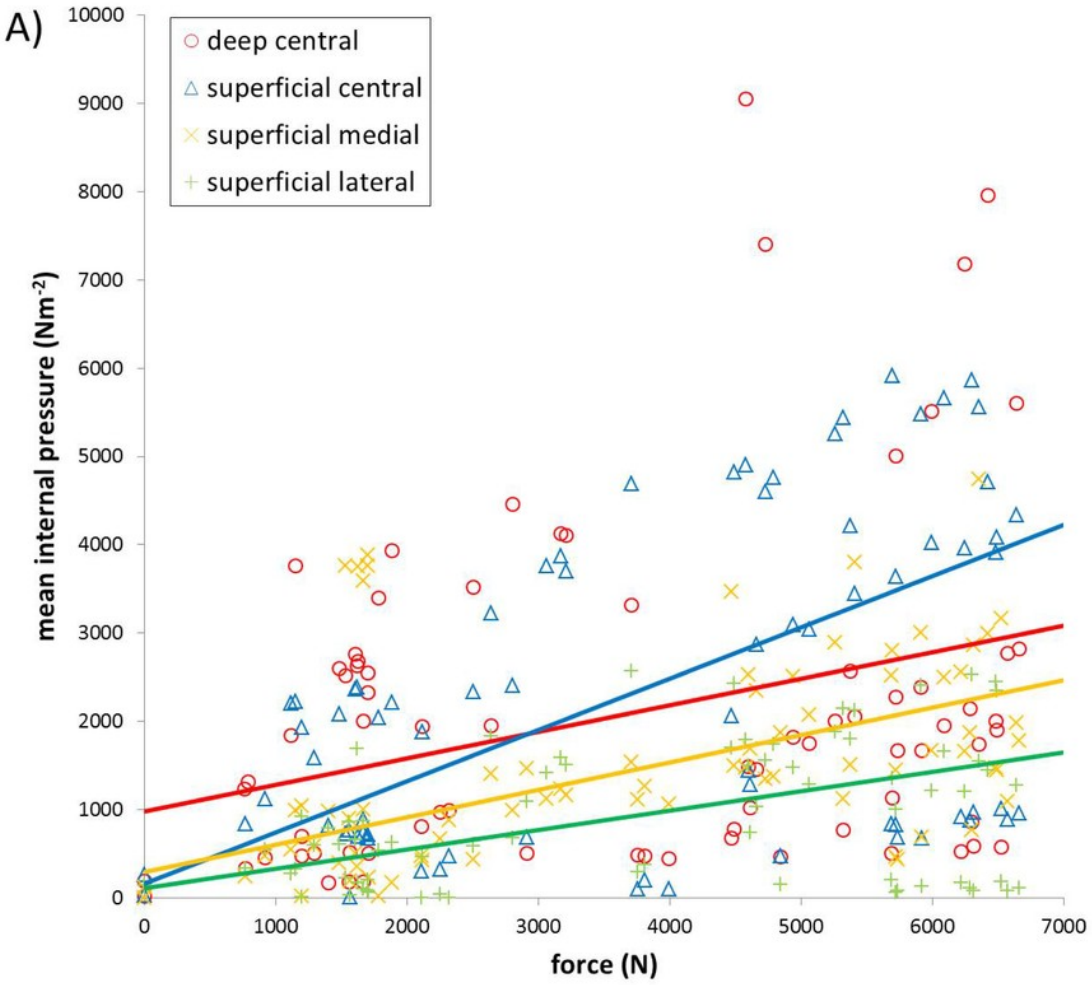


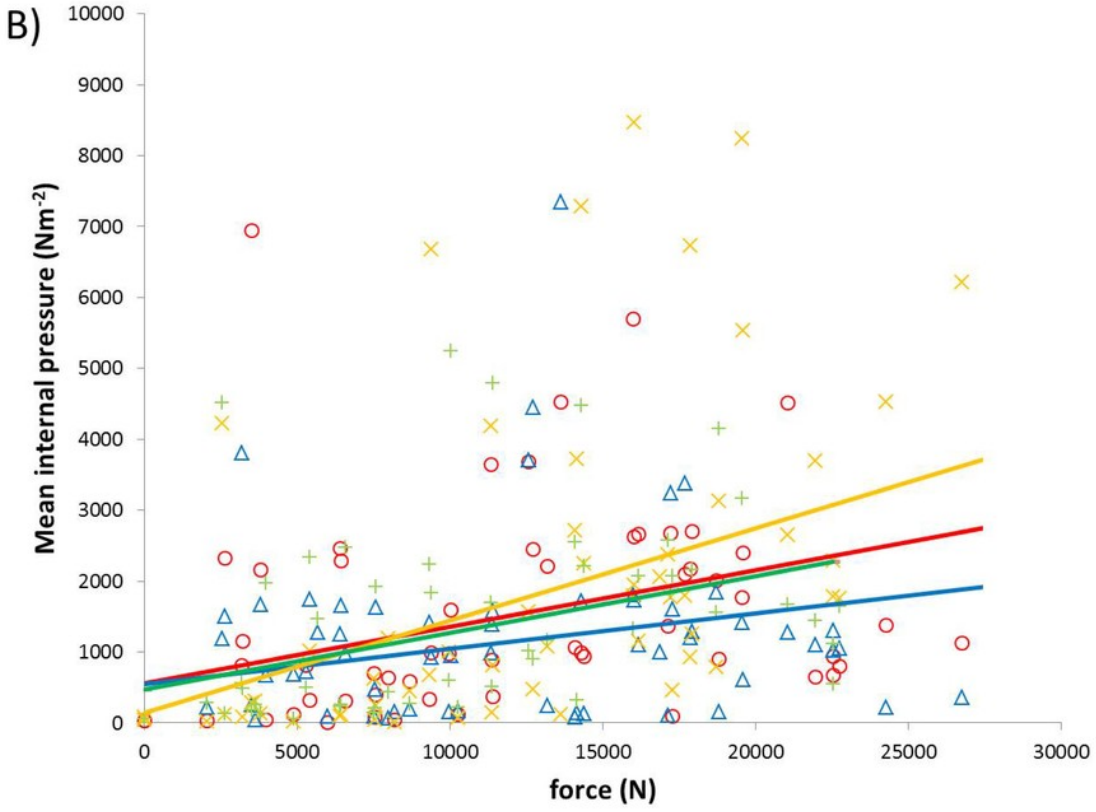

# Figure 11

Species comparison: mean internal pressure in each digital cushion (DC) region.

A) Deep central, B) superficial central, C) superficial medial, D) superficial lateral. Triangles with the solid (LMER) line denote horse data, circles with the dashed (LMER) line denotes elephant data. P values show whether the slopes of the lines are significantly different between taxa.

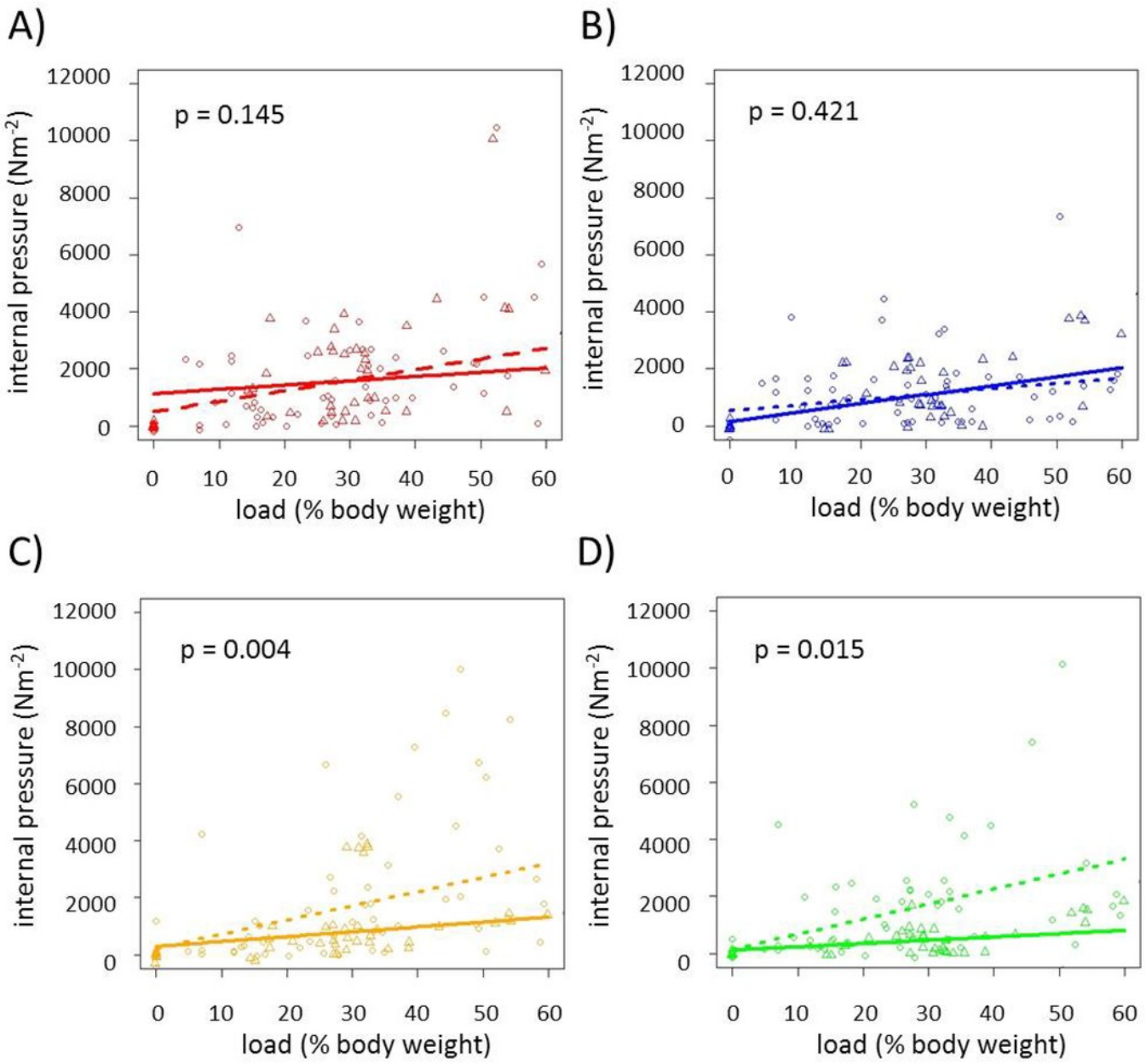




*PeerJ PrePrints* | http://dx.doi.org/10.7287/peerj.preprints.231v1 | CC-BY 4.0 Open Access | received: 2 Feb 2014, published: 2 Feb 2014

# Table 1(on next page)

Subject information.

Missing information is unknown. Details of the gross pathologies evident in elephant limbs are in Data S1. Asterisks (*) denote that the value is estimated (e.g. Miller *et al*., 2008, or by post-mortem staff, based on relative stature of the horse).



*PeerJ PrePrints* | http://dx.doi.org/10.7287/peerj.preprints.231v1 | CC-BY 4.0 Open Access | received: 2 Feb 2014, published: 2 Feb 2014

| subject | limb | breed | age | shoulder height (cm) | body weight (kg) | foot circumference (cm) | surface area ($cm^2$) | gross pathology evident |
|---|---|---|---|---|---|---|---|---|
| Elephant 1 | RF | Asian | | 293* | 3000* | 130 | 1202 | yes |
| Elephant 2 | RF | Asian | 17 | 293 | 3000* | 133 | 1252 | no |
| Elephant 3 | RF | Asian | 55 | 386* | 3960 | 142 | 1401 | yes |
| Elephant 4 | LF | African | | 244* | 2500* | 112 | 908 | yes |
| Elephant 5 | RF | African | 32 | 300* | 3500* | 132 | 1222 | no |
| Elephant 6 | LF | Asian | 39 | 290 | 5500 | 140 | 1378 | no |
| Horse 1 | RF | mixed | 19 | 122* | 700* | 44 | 131 | no |
| Horse 2 | RF | mixed | 20 | 78* | 450* | 50 | 169 | no |
| Horse 3 | RF | mixed | 25 | 78* | 450* | 47 | 137 | no |
| Horse 4 | LF | mixed | | 96* | 550 | 47 | 160 | no |
| Horse 5 | LF | mixed | | 113 | 650 | 57 | 207 | no |
| Horse 6 | LF | mixed | 5 | 109 | 536 | 50 | 180 | no |
| Horse 7 | RF | mixed | 4 | 105* | 602 | 53 | 197 | no |

## Table 2(on next page)

Results of the LMER analysis (see Methods).

Mean and maximum instantaneous internal pressure in both species. y = mx + c, where y is pressure ($Nm^{-2}$) and x is force (N). * denotes the values is significantly different from zero, p values for the slope (m) are shown.

| | Mean Internal Pressure | | | | | | Max. Inst. Internal Pressure | | | | | |
|---|---|---|---|---|---|---|---|---|---|---|---|---|
| | Horse | | | Elephant | | | Horse | | | Elephant | | |
| | intercept | slope | p | intercept | slope | p | intercept | slope | p | intercept | slope | p |
| deep central (d.c.) | 980* | 0.30* | 0.004 | 556 | 0.08* | 0.008 | 1334* | 0.28* | 0.004 | 943 | 0.09 | 0.176 |
| sup. central (s.c.) | 164 | 0.58* | < 0.001 | 547 | 0.05* | 0.048 | 255 | 0.59* | < 0.001 | 495 | 0.10* | 0.016 |
| sup. medial (s.m.) | 113 | 0.22* | < 0.001 | 144 | 0.13* | 0.002 | 72 | 0.28* | < 0.001 | -91 | 0.29* | 0.007 |
| sup. lateral (s.l.) | 293 | 0.31* | < 0.001 | 474 | 0.08* | 0.002 | 384 | 0.32* | < 0.001 | 481 | 0.10* | 0.002 |

## Table 3(on next page)

Mean internal pressure.

Comparing linear coefficients from the LMER analysis for each DC location. Pressures that are significantly different are emphasised in bold.

| | Horse | | | | Elephant | | | |
|---|---|---|---|---|---|---|---|---|
| | d.c. | s.c. | s.m. | s.l. | d.c. | s.c. | s.m. | s.l. |
| deep central (d.c.) | | 0.718 | **<0.001** | **<0.001** | | 0.161 | **0.002** | 0.183 |
| sup. central (s.c.) | 0.718 | | **<0.001** | **<0.001** | 0.161 | | **<0.001** | 0.107 |
| sup. medial (s.m.) | **<0.001** | **<0.001** | | **0.001** | **0.002** | **<0.001** | | **0.011** |
| sup. lateral (s.l.) | **<0.001** | **<0.001** | **0.001** | | 0.760 | 0.107 | **0.011** | |

## Table 4(on next page)

Maximum instantaneous internal pressure.

Comparing linear coefficients from the LMER analysis for each DC location. Pressures that are significantly different are emphasised in bold.

| | Horse | | | | Elephant | | | |
|---|---|---|---|---|---|---|---|---|
| | d.c. | s.c. | s.m. | s.l. | d.c. | s.c. | s.m. | s.l. |
| deep central (d.c.) | | 0.778 | **<0.001** | **<0.001** | | 0.611 | **<0.001** | 0.866 |
| sup. central (s.c.) | 0.778 | | **<0.001** | **<0.001** | 0.611 | | **<0.001** | 0.520 |
| sup. medial (s.m.) | **<0.001** | **<0.001** | | 0.126 | **<0.001** | **<0.001** | | **<0.001** |
| sup. lateral (s.l.) | **<0.001** | **<0.001** | 0.126 | | 0.866 | 0.520 | **<0.001** | |

# Table 5(on next page)

Previously reported external palmar foot pressures.

Mean values are shown during walking (N.B. speed was not controlled in these studies).



*PeerJ PrePrints* | http://dx.doi.org/10.7287/peerj.preprints.231v1 | CC-BY 4.0 Open Access | received: 2 Feb 2014, published: 2 Feb 2014

| | Horse | Elephant |
|---|---|---|
| max *in vivo* pressure ($kNm^{-2}$) | 460.4[b] | 62.5[a] |
| predicted peak palmar pressure ($kNm^{-2}$) (using $M^{0.5}$) | 237.3[c] | 594.3[c] |

All values are means.

[a] Panagiotopoulou *et al.,* 2012; [b]Oosterlink *et al.,* 2011; [c] Michilsens *et al.,* 2009.

## Table 6(on next page)

Results for external palmar pressures.

Palmar surface area was determined manually using foot circumference, and contact surface area was calculated from the number of sensors with values > 0 $Ncm^{-2}$ from the pressure pad. The ratio of foot cross sectional areas (foot CSA): digital cushion cross sectional area (DC CSA) was calculated from axial CT data at the level of the needles. All values are median (± IQR).

| | Horse | Elephant |
|---|---|---|
| Palmar surface area ($m^2$) | 0.017 (0.004) | 0.124 (0.014) |
| Contact surface area ($m^2$) | 0.005 (0.003) | 0.056 (0.036) |
| Ratio palmar surface area : contact surface area | 3.38 (2.18) | 2.34 (1.83) |
| Ratio foot CSA: DC CSA | 5.09 (1.09) | 3.09 (1.08) |
| Mean *ex vivo* external pressures ~30% BW ($kNm^{-2}$) | 7.2 (6.6) | 4.3 (1.1) |
| Max. *ex vivo* external pressures ~30% BW ($kNm^{-2}$) | 63.0 (23.0) | 36.0 (102.0) |